

# Estimating Phosphorescent Emission Energies in Ir(III) Complexes using Large-Scale Quantum Computing Simulations

Scott N. Genin,<sup>\*,†</sup> Ilya G. Ryabinkin,<sup>†</sup> Nathan R. Paisley,<sup>‡</sup> Sarah O. Whelan,<sup>†</sup>

Michael G. Helander,<sup>†</sup> and Zachary M. Hudson<sup>\*,‡</sup>

<sup>†</sup>*OTI Lumionics Inc., 100 College St. #351, Toronto, Ontario M5G 1L5, Canada*

<sup>‡</sup>*Department of Chemistry, The University of British Columbia, 2036 Main Mall, Vancouver, British Columbia V6T 1Z1, Canada*

E-mail: [scott.genin@otilumionics.com](mailto:scott.genin@otilumionics.com); [zhudson@chem.ubc.ca](mailto:zhudson@chem.ubc.ca)

## Abstract

Quantum chemistry simulations that accurately predict the properties of materials are among the most highly anticipated applications of quantum computing. It is widely believed that simulations running on quantum computers will allow for higher accuracy, but there has not yet been a convincing demonstration that quantum methods are competitive with existing classical methods at scale. Here we apply the iterative qubit coupled cluster (iQCC) method on classical hardware to the calculation of the  $T_1 \rightarrow S_0$  transition energies in nine phosphorescent iridium complexes, to determine if quantum simulations have any advantage over traditional computing methods. Phosphorescent iridium complexes are integral to the widespread commercialization of organic light-emitting diode (OLED) technology, yet accurate computational prediction of their emission energies remains a challenge. Our simulations would require a gate-based quantum computer with a minimum of 72 fully-connected and error-corrected logical

qubits. Since such devices do not yet exist, we demonstrate the iQCC quantum method using a special purpose quantum simulator on classical hardware. The results are compared to a selection of common density-functional theory (DFT) functionals (B3LYP, CAM-B3LYP, LC-wHPBE), *ab initio* methods (HF and MP2), and experimental data. The iQCC quantum method is found to match the accuracy of the fine-tuned DFT functionals, has a better Pearson correlation coefficient, and still has considerable potential for systematic improvement. Based on these results, we anticipate that the iQCC quantum method will have the required accuracy to design organometallic complexes when deployed on emerging quantum hardware.

## Introduction

Computational chemistry methods such as quantum chemistry simulations are becoming increasingly important tools for chemical, material, and molecular design. Whether simulating molecular docking in pharmaceuticals or the optical gaps of semiconductors, simulations underpin several multi-trillion-dollar chemical and material industries.<sup>1-4</sup> Results from simulations are typically either used to screen potential candidates for desired properties, or used to train predictive machine learning models.<sup>5-8</sup> In either case, robust and accurate quantum chemistry methods are needed to reliably predict structure-property relationships in order to progress from use in rough screening towards precision *in silico* design. However, the exact solution to the electronic Schrödinger equation, known as the full configurational interaction (FCI), scales exponentially with system size and is thus intractable for all but the smallest molecules. To resolve this issue, many approximate methods have been developed that are either *ab initio* or semi-empirical. Density-functional theory (DFT) is one of the most used types of quantum chemistry simulation, but often requires fine-tuning of the functionals to achieve a high level of accuracy. Furthermore, DFT often performs poorly for more complex systems with higher degrees of electron correlation, particularly when trying to simulate excited or transition states.<sup>9</sup> New quantum chemistry methods capable of accurately

simulating electron correlation energies without first tuning parameters for a specific problem are thus highly desirable and are an active area of research.

Quantum computers, which operate using quantum states of matter, have recently attracted major research interest as potential new tools for high-accuracy quantum chemistry simulations.<sup>10–13</sup> The largest quantum chemistry simulation to date on a quantum computer was limited to a Hartree–Fock simulation of  $\text{H}_{12}$  and diazene using 12 logical qubits,<sup>14</sup> problems that are otherwise straightforward to simulate on a classical computer. It is not yet possible to perform a quantum chemistry simulation that is difficult (or impossible) to solve on a classical computer, using current noisy intermediate-scale quantum (NISQ) computers. It has been postulated that a quantum computer with 50–100 logical qubits (or  $\sim 10^2$ – $10^4$  physical qubits depending on the error correction scheme<sup>15</sup>) would provide quantum advantage over a classical computer for quantum chemistry problems.<sup>16,17</sup> At this scale, a quantum computer could potentially enable accurate quantum chemistry simulations of small molecules that are large enough to be commercially relevant in a variety of industries, and that are otherwise known to be difficult to simulate with traditional methods, such as organometallic complexes.

The electronic structure of late transition metal complexes are known to be difficult to accurately simulate due to the large number of orbitals, the challenge in modeling electron correlation, and the relativistic effects of the metal centre.<sup>18</sup> Nonetheless, these complexes are important to multiple industries, for example as catalysts, semiconductor precursors, pharmaceuticals and as phosphorescent emitters for organic light-emitting diodes (OLEDs). Cyclometalated iridium (III) complexes are common emitters used commercially in OLED displays and lighting, due to their high quantum yield and short radiative triplet lifetimes.<sup>19–22</sup> The phosphorescent emission colors of these complexes are determined by the triplet-to-singlet ( $T_1 \rightarrow S_0$ ) transition, making this an ideal problem for testing new quantum chemistry simulations, since these transitions i) can easily be measured experimentally with high reproducibility; ii) require the simulation of both ground and excited states, and iii)

have been extensively studied using DFT<sup>23,24</sup> and time-dependent density-functional theory (TDDFT).<sup>25,26</sup> These transitions are known to be difficult problems to simulate, as DFT methods commonly have an error of  $\sim 0.3$  eV,<sup>27</sup> which is sufficient as a rough screening tool, but not for precision *in silico* design. While DFT functionals can be fine-tuned for a particular system to improve accuracy, choosing an optimal functional is a daunting task due to the number of functionals available.

Unfortunately, at the time of writing, a quantum computer with enough qubits and sufficient error rate suitable for simulating the  $T_1 \rightarrow S_0$  transition in phosphorescent emitters does not yet exist. Nonetheless, to test if quantum chemistry simulations on a quantum computer could provide any advantage for this class of problems, we performed simulations using the iterative qubit coupled cluster (iQCC) quantum method on a classical computer.<sup>28–30</sup> The iQCC method formulates the electronic structure problem natively in qubit space in a highly efficient manner and was originally designed to overcome many of the hardware limitations of today’s NISQ quantum computers. As a result of iQCC’s highly efficient formulation, problems that would otherwise require too many quantum gate operations to practically solve on a classical computer can still be solved using modest classical hardware. In effect, our iQCC quantum-on-classical-hardware simulations are emulating the capabilities of a future quantum computer using classical hardware available today. This approach has the advantage of having full qubit connectivity and no error, while also facilitating large-scale calculations that cannot be run on currently available quantum computers. Using the iQCC quantum simulator, we evaluate whether a quantum computer could accurately simulate the  $T_1 \rightarrow S_0$  transition in phosphorescent emitters and whether this approach has any advantages to existing classical methods such as DFT.

## Results and discussion

The geometry of nine cyclometalated Ir(III) complexes, see Fig. 1 were first optimized at

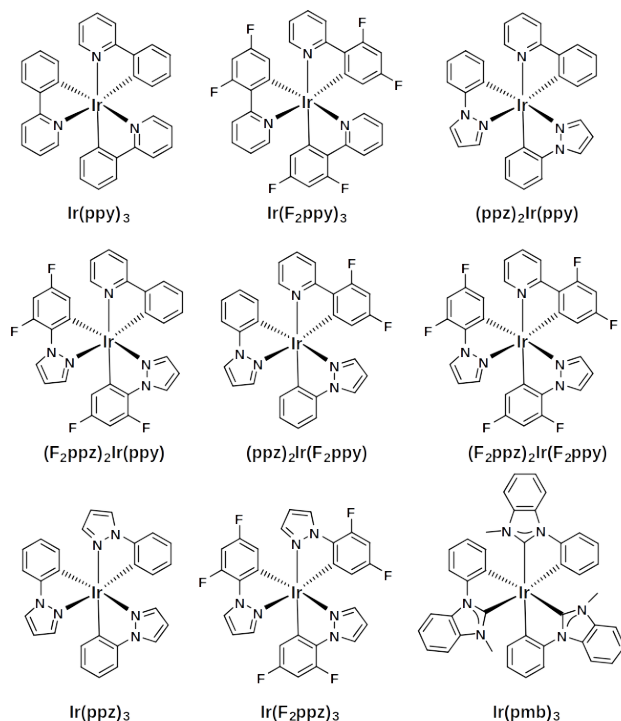


Figure 1: The nine cyclometalated Ir(III) complexes simulated here.

$T_1$  state using the range-separated DFT functional, CAM-B3LYP<sup>31</sup> with the LANL2def-DZV basis set<sup>32,33</sup> with unrestricted Hartree–Fock orbitals. Singlet and triplet states were subsequently simulated using several *ab initio*, DFT, and TDDFT simulations. The *ab initio* low-scaling Hartree–Fock and second-order Møller–Plesset perturbation theory (MP2) methods were used, as well as well-known DFT functionals (B3LYP)<sup>34</sup> and range-separated DFT functionals (CAM-B3LYP and LC-wHPBE)<sup>35</sup> with both LANL2def-dzv and SBKJC-ECP 6-31G\* basis sets.<sup>36</sup> TDDFT simulations of the triplet states with the same functionals were run with and without the Tamm-Dancoff approximation.<sup>37</sup> The optimized triplet state geometries were used to carry out spin-restricted open-shell Hartree–Fock molecular orbital (MO) calculations to generate the values of one- and two- electron integrals using a modified version of GAMESS.<sup>38,39</sup> 18 occupied and 18 unoccupied Hartree–Fock MOs below and above the Fermi level constitute a complete active space (CAS) containing 36 active electrons over 36 active spin orbitals. The one- and two-electron integrals from the CAS(36,36) were used to construct the qubit Hamiltonian for iQCC using the Jordan-Wigner transformation.<sup>40</sup> The

iQCC quantum simulator was used to solve for the converged  $T_1$  and  $S_0$  energies applying corrections from perturbation theory (PT)<sup>28–30</sup> (Fig. 2). Here, the PT correction refers specifically to Epstein-Nesbet perturbation theory, which applies a perturbative correction to the iQCC energy.<sup>30</sup> These results are equivalent to those that would be produced using a quantum computer with 72 *logical* qubits, and which is within the range of problem size where a quantum advantage has been postulated.<sup>41</sup>

The iQCC method has been improved upon since its disclosure in earlier reports, as described in the supplementary information. The iQCC method was originally developed to enable flexibility in quantum circuit depth by allowing an Ansatz, or quantum instruction set, to be partitioned and optimized independently.<sup>29</sup> The Ansatz is then incorporated or “dressed” into the Hamiltonian for the next step (SI Eq. 16). Since the Ansatz does not fully commute with the Hamiltonian, the incorporation results in additional terms being added into the Hamiltonian, with exponential growth proportional to  $(3/2)^N$ , but in every case the growth plateaued, enabling efficient scaling of the iQCC quantum simulator on classical hardware for these problems (Fig. 2c).

The mean accuracy of the iQCC+PT simulations for the set of Ir complexes was superior to nearly all of the studied DFT and *ab initio* methods for simulating the  $T_1 \rightarrow S_0$  transition for this set of complexes. Only the fine-tuned LC-wHPBE functionals produced energies with lower mean absolute error, although with higher standard deviation (Fig. 3). All methods tested showed variations from the experimental value, attributable to the approximations and/or intrinsic errors inherent to each method. The absence of solvation effects and the use of double-zeta basis sets are likely the two largest sources of error across all methods. The current limitations of the iQCC and iQCC+PT results can be attributed to the limited CAS size used, which was selected for practical consideration. At this size, the total number of all possible electronic configurations (of any spin) is  $\binom{36}{18}^2 \approx 10^{20}$ . Apparently, a problem too large for using the FCI method on a classical computer. The CAS limitation results in the treatment of electrons and orbitals outside of the CAS only at the mean-field level, so there

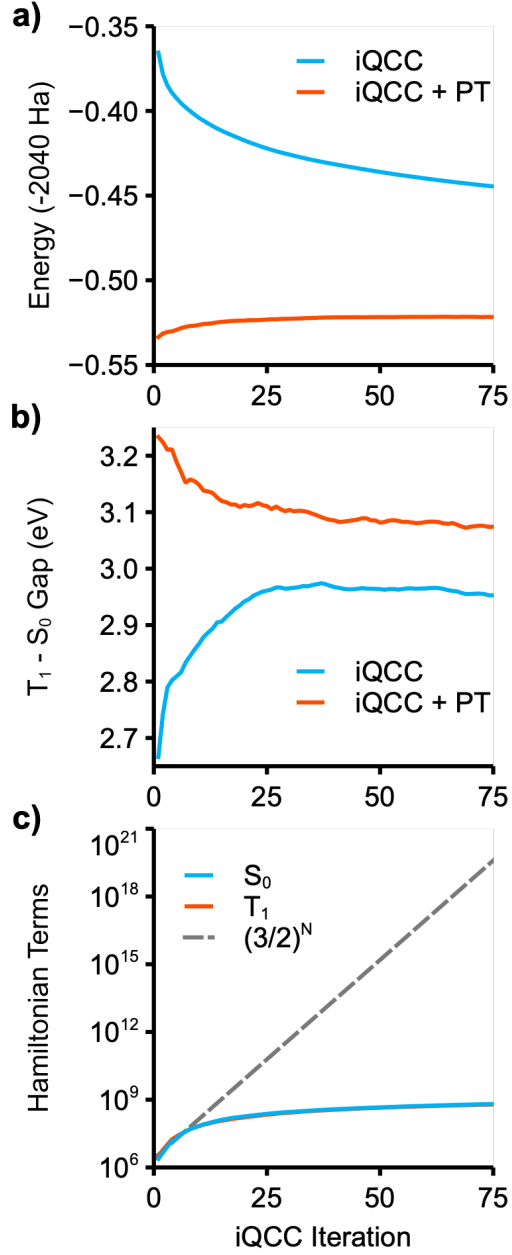


Figure 2: Representative convergence curves for Ir(pmb)<sub>3</sub> with iQCC and iQCC + PT  $E_h$  for the  $S_0$  state (scale minimum is  $-2040.55 E_h$ ), b)  $T_1$ - $S_0$  gap in eV plotted per iQCC iteration for both iQCC and iQCC + PT, and c) Hamiltonian term size with respect to iQCC iteration for both  $S_0$  and  $T_1$  for Ir(pmb)<sub>3</sub>, including a line to show the theoretical Hamiltonian term growth.

is an implicit assumption the electron correlation outside of the CAS is not significant.

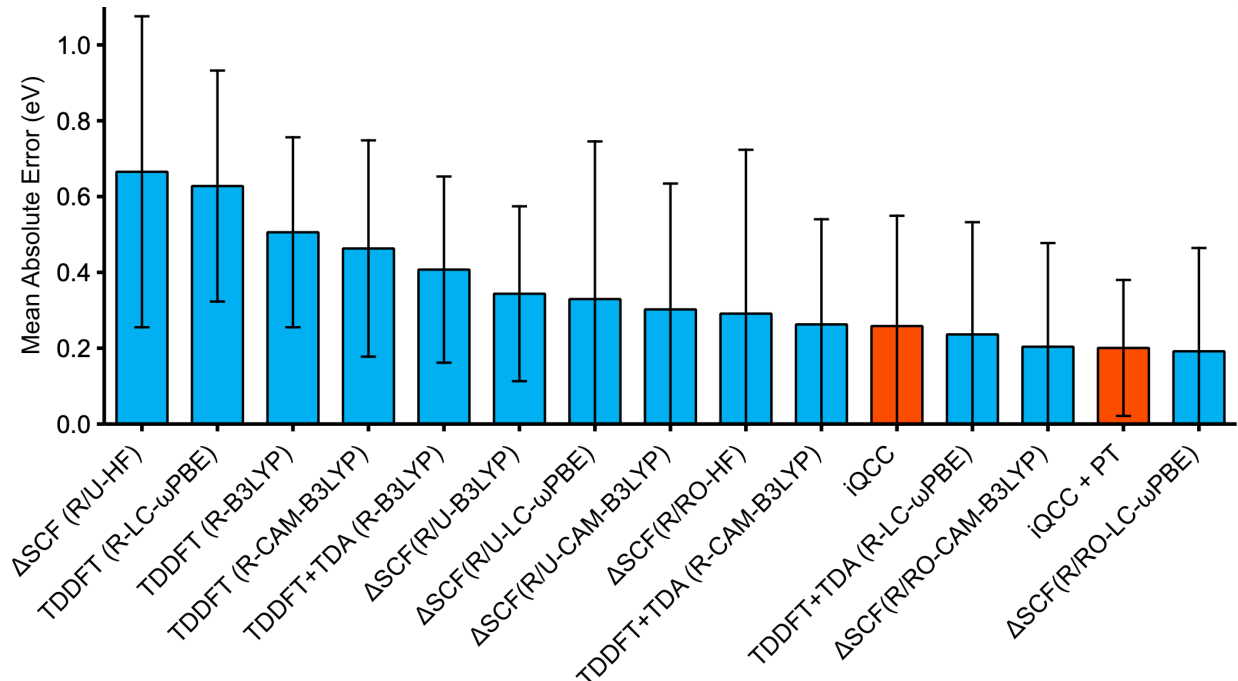


Figure 3: Mean absolute deviations from experimental data for the different electronic structure methods. Error bars indicate the standard deviation. Experimental  $T_1$ - $S_0$  energies were obtained at 77 K in dilute frozen 2-MeTHF solution.<sup>20</sup>

The best-performing DFT functionals for this set were the long-range corrected functionals LC- $\omega$ HPBE and CAM-B3LYP when using restricted open shell orbitals, however when using unrestricted orbitals, the B3LYP, CAM-B3LYP and LC- $\omega$ HPBE had very similar average values. The common DFT functional PBE was also tested using restricted open shell orbitals and showed a much larger absolute deviation (1.437 eV compared to  $\sim 0.2$  eV for CAM-B3LYP and LC- $\omega$ HPBE) and is thus not shown below. There was also a large range in error for the *ab initio* methods; while MP2 is often considered to be more accurate than HF, this was not the case here (SI table). The PT correction introduced a blue shift to the  $T_1 \rightarrow S_0$  transition on average of 0.3 eV with a range of 0.04-0.72 eV, resulting in 7 of the 9 Ir (III) complexes examined showing a blue shift in phosphorescence emission relative to experiment. This outcome was expected based on the absence of solvent and thermal effects in the simulations, which would be expected to red-shift the experimental values.



To be useful as a precision *in silico* design tool, it is important that a method can correctly predict structure-property relationships, or in other words the correlation between changes in chemical structure and changes in electronic structure. It was found that the iQCC and iQCC+PT results have higher Pearson’s correlation coefficients than even those using the LC-wHPBE functional, and that the iQCC+PT is significant at the 95% confidence interval (Table 1). This implies that iQCC+PT is more accurate at predicting the structure-property relationship and could potentially be a more useful tool for chemical design compared to the best-performing DFT methods examined.

Table 1: Mean average deviation (eV), standard deviation (eV), Pearson’s correlation coefficients (higher is better) and P-values (closer to 0 is better) for the best performing methods.

Method	Mean average deviation, eV	Standard deviation, eV	Pearson	P-value
ROHF/RHF	0.291	0.432	−0.413	0.269
ROMP2/RMP2 <sup>1</sup>	0.246	0.390	0.438	0.276
RO/R LC-wHPBE	0.192	0.272	0.328	0.388
TDDFT+TDA, LC-wHPBE	0.236	0.296	0.255	0.507
iQCC	0.258	0.291	0.522	0.149
iQCC + PT	0.201	0.179	0.762	0.018

<sup>1</sup> An outlier data point was removed for R/RO-MP2 for Ir(ppy)<sub>3</sub>, gap = 8.9 eV

In summary, nine cyclometalated Ir (III) complexes were calculated using the iQCC method using a special purpose quantum simulator that emulates a quantum computer with 72 logical qubits. The results are found to be competitive with, or superior to, many leading DFT and *ab initio* methods, when compared to experimental data. Specifically, the iQCC method combined with PT corrections is found to match the accuracy of fine-tuned DFT functionals for simulating the  $T_1 \rightarrow S_0$  transition, but with more accurate prediction of the structure-property relationship. This implies that the iQCC quantum method has the potential to be robust and reliable enough to simulate a set of materials without parameter tuning, which will be beneficial to the design of *de novo* materials when experimental data

is not widely available. These results show that a quantum computer with fully connected and error-corrected qubits will be capable of accurately simulating chemical properties, and provides an optimistic view on the future of quantum methods for chemical design. Finally, the iQCC quantum-on-classical-hardware simulations demonstrated here are not limited to just simulation of the  $T_1 \rightarrow S_0$  transition in phosphorescent emitters and has already been successfully used to simulate other chemical systems and properties, the results of which will be published elsewhere.

## References

- (1) Marzari, N.; Ferretti, A.; Wolverton, C. Electronic-structure methods for materials design. *Nat. Mater.* **2021**, *20*, 736–749.
- (2) Jorgensen, W. L. The Many Roles of Computation in Drug Discovery. *Science* **2004**, *303*, 1813–1818.
- (3) Liu, H.; Naumov, I. I.; Hoffmann, R.; Ashcroft, N. W.; Hemley, R. J. Potential high- $T_c$  superconducting lanthanum and yttrium hydrides at high pressure. *Proc. Natl. Acad. Sci. USA* **2017**, *114*, 6990–6995.
- (4) Ackland, G. J.; Dunuwille, M.; Martinez-Canales, M.; Loa, I.; Zhang, R.; Sinogeikin, S.; Cai, W.; Deemyad, S. Quantum and isotope effects in lithium metal. *Science* **2017**, *356*, 1254–1259.
- (5) Nandy, A.; Duan, C.; Janet, J. P.; Gugler, S.; Kulik, H. J. Strategies and Software for Machine Learning Accelerated Discovery in Transition Metal Chemistry. *Ind. Eng. Chem. Res.* **2018**, *57*, 13973–13986.
- (6) Joung, J. F.; Han, M.; Hwang, J.; Jeong, M.; Choi, D. H.; Park, S. Deep Learning Optical Spectroscopy Based on Experimental Database: Potential Applications to Molecular Design. *JACS Au* **2021**, *1*, 427–438.

- (7) Moosavi, S. M.; Jablonka, K. M.; Smit, B. The Role of Machine Learning in the Understanding and Design of Materials. *J. Am. Chem. Soc.* **2020**, *142*, 20273–20287, PMID: 33170678.
- (8) Fanourgakis, G. S.; Gkagkas, K.; Tylianakis, E.; Froudakis, G. E. A Universal Machine Learning Algorithm for Large-Scale Screening of Materials. *J. Am. Chem. Soc.* **2020**, *142*, 3814–3822, PMID: 32017547.
- (9) Becke, A. D. Perspective: Fifty years of density-functional theory in chemical physics. *J. Chem. Phys.* **2014**, *140*, 18A301.
- (10) Feynman, R. P. Simulating physics with computers. *Int. J. Theor. Phys.* **1982**, *21*, 467–488.
- (11) Lloyd, S. Universal Quantum Simulators. *Science* **1996**, *273*, 1073–1078.
- (12) Abrams, D. S.; Lloyd, S. Simulation of Many-Body Fermi Systems on a Universal Quantum Computer. *Phys. Rev. Lett.* **1997**, *79*, 2586–2589.
- (13) Ladd, T. D.; Jelezko, F.; Laflamme, R.; Nakamura, Y.; Monroe, C.; O’Brien, J. L. Quantum computers. *Nature* **2010**, *464*, 45–53.
- (14) Google AI Quantum and Collaborators, et al. Hartree-Fock on a superconducting qubit quantum computer. *Science* **2020**, *369*, 1084–1089.
- (15) Fowler, A. G.; Mariantoni, M.; Martinis, J. M.; Cleland, A. N. Surface codes: Towards practical large-scale quantum computation. *Phys. Rev. A* **2012**, *86*, 032324.
- (16) Arute, F.; Arya, K.; Babbush, R.; Bacon, D.; Bardin, J. C.; Barends, R.; Biswas, R.; Boixo, S.; Brandao, F. G. S. L.; Buell, D. A.; et al. Quantum supremacy using a programmable superconducting processor. *Nature* **2019**, *574*, 505–510.

- (17) Bochevarov, V. E. E.; Broer, B. W.; Webber, M.; Gavartin, J.; Halls, M. D.; Lorton, K. P.; A., How will quantum computers provide an industrially relevant computational advantage in quantum chemistry? online, 2020.
- (18) Nandy, A.; Duan, C.; Taylor, M. G.; Liu, F.; Steeves, A. H.; Kulik, H. J. Computational Discovery of Transition-metal Complexes: From High-throughput Screening to Machine Learning. *Chem. Rev.* **2021**, *121*, 9927–10000.
- (19) Lamansky, S.; Djurovich, P.; Murphy, D.; Abdel-Razzaq, F.; Lee, H.-E.; Adachi, C.; Burrows, P. E.; Forrest, S. R.; Thompson, M. E. Highly Phosphorescent Bis-Cyclometalated Iridium Complexes: Synthesis, Photophysical Characterization, and Use in Organic Light Emitting Diodes. *J. Am. Chem. Soc.* **2001**, *123*, 4304–4312.
- (20) Sajoto, T.; Djurovich, P. I.; Tamayo, A. B.; Oxgaard, J.; Goddard, W. A.; Thompson, M. E. Temperature Dependence of Blue Phosphorescent Cyclometalated Ir(III) Complexes. *J. Am. Chem. Soc.* **2009**, *131*, 9813–9822.
- (21) Lai, P.-N.; Brysacz, C. H.; Alam, M. K.; Ayoub, N. A.; Gray, T. G.; Bao, J.; Teets, T. S. Highly Efficient Red-Emitting Bis-Cyclometalated Iridium Complexes. *J. Am. Chem. Soc.* **2018**, *140*, 10198–10207.
- (22) You, Y.; Park, S. Y. Phosphorescent iridium(iii) complexes: toward high phosphorescence quantum efficiency through ligand control. *Dalton Trans.* **2009**, 1267–1282.
- (23) Hohenberg, P.; Kohn, W. Inhomogeneous Electron Gas. *Phys. Rev.* **1964**, *136*, B864.
- (24) Kohn, W.; Sham, L. J. Self-Consistent Equations Including Exchange and Correlation Effects. *Phys. Rev.* **1965**, *140*, A1133.
- (25) Runge, E.; Gross, E. K. U. Density-Functional Theory for Time-Dependent Systems. *Phys. Rev. Lett.* **1984**, *52*, 997–1000.

- (26) Bowler, D. R.; Miyazaki, T. Calculations for millions of atoms with density functional theory: linear scaling shows its potential. *J. Phys. Condens. Matter* **2010**, *22*, 074207.
- (27) Horbatenko, Y.; Lee, S.; Filatov, M.; Choi, C. H. Performance Analysis and Optimization of Mixed-Reference Spin-Flip Time-Dependent Density Functional Theory (MRSF-TDDFT) for Vertical Excitation Energies and Singlet–Triplet Energy Gaps. *J. Phys. Chem. A* **2019**, *123*, 7991–8000.
- (28) Ryabinkin, I. G.; Yen, T.-C.; Genin, S. N.; Izmaylov, A. F. Qubit Coupled Cluster Method: A Systematic Approach to Quantum Chemistry on a Quantum Computer. *J. Chem. Theory Comput.* **2018**, *14*, 6317–6326.
- (29) Ryabinkin, I. G.; Lang, R. A.; Genin, S. N.; Izmaylov, A. F. Iterative Qubit Coupled Cluster Approach with Efficient Screening of Generators. *J. Chem. Theory Comput.* **2020**, *16*, 1055–1063, PMID: 31935085.
- (30) Ryabinkin, I. G.; Izmaylov, A. F.; Genin, S. N. A posteriori corrections to the iterative qubit coupled cluster method to minimize the use of quantum resources in large-scale calculations. *Quantum Sci. Technol.* **2021**, *6*, 024012.
- (31) Yanai, T.; Tew, D. P.; Handy, N. C. A new hybrid exchange-correlation functional using the Coulomb-attenuating method (CAM-B3LYP). *Chem. Phys. Lett.* **2004**, *393*, 51–57.
- (32) Hay, P. J.; Wadt, W. R. Ab initio effective core potentials for molecular calculations. Potentials for K to Au including the outermost core orbitals. *J. Chem. Phys.* **1985**, *82*, 299–310.
- (33) Roy, L. E.; Hay, P. J.; Martin, R. L. Revised Basis Sets for the LANL Effective Core Potentials. *J. Chem. Theory Comput.* **2008**, *4*, 1029–1031, PMID: 26636355.
- (34) Becke, A. D. Density-functional thermochemistry. III. The role of exact exchange. *J. Chem. Phys.* **1993**, *98*, 5648–5652.

- (35) Vydrov, G. E., Oleg A .and Scuseria Assessment of a long-range corrected hybrid functional. *J. Chem. Phys.* **2006**, *125*, 234109.
- (36) Stevens, W. J.; Krauss, M.; Basch, H.; Jasien, P. G. Relativistic compact effective potentials and efficient, shared-exponent basis sets for the third-, fourth-, and fifth-row atoms. *Can. J. Chem.* **1992**, *70*, 612–630.
- (37) Peach, M. J. G.; Williamson, M. J.; Tozer, D. J. Influence of Triplet Instabilities in TDDFT. *J. Chem. Theory Comput.* **2011**, *7*, 3578–3585.
- (38) Schmidt, M. W.; Baldridge, K. K.; Boatz, J. A.; Elbert, S. T.; Gordon, M. S.; Jensen, J. H.; Koseki, S.; Matsunaga, N.; Nguyen, K. A.; Su, S. J.; Windus, T. L.; Dupuis, M.; Montgomery, J. General Atomic and Molecular Electronic Structure System. *J. Comput. Chem.* **1993**, *14*, 1347–1363.
- (39) Gordon, M. S.; Schmidt, M. W. In *Theory and Applications of Computational Chemistry. The first forty years*; Dykstra, C. E., Frenking, G., Kim, K. S., Scuseria, G. E., Eds.; Elsevier: Amsterdam, 2005; pp 1167–1189.
- (40) Nielsen, M. A. The Fermionic canonical commutation relations and the Jordan–Wigner transform. *School of Physical Sciences The University of Queensland* **2005**,
- (41) Yuan, X. A quantum-computing advantage for chemistry. *Science* **2020**, *369*, 1054–1055.

# Supplementary Information for

## Estimating Phosphorescent Emission Energies in

## Ir(III) Complexes using Large-Scale Quantum

## Computing Simulations

Scott N. Genin,<sup>\*,†</sup> Ilya G. Ryabinkin,<sup>†</sup> Nathan R. Paisley,<sup>‡</sup> Sarah O. Whelan,<sup>†</sup>  
Michael G. Helander,<sup>†</sup> and Zachary M. Hudson<sup>\*,‡</sup>

<sup>†</sup>*OTI Lumionics Inc., 100 College St. #317 (Material Discovery), Toronto, Ontario  
M5G 1L5, Canada*

<sup>‡</sup>*Department of Chemistry, The University of British Columbia, 2036 Main Mall, Vancouver,  
British Columbia V6T 1Z1, Canada*

E-mail: [scott.genin@otilumionics.com](mailto:scott.genin@otilumionics.com); [zhudson@chem.ubc.ca](mailto:zhudson@chem.ubc.ca)

Phone: +1 (604) 822-3266. Fax: +1 (604) 822-2847

## S1 The iterative qubit coupled cluster (iQCC) method

### S1.1 Second-quantized electronic Hamiltonian

The qubit coupled cluster (QCC) method starts from a second-quantized electronic Hamiltonian of a molecule:<sup>1-4</sup>

$$\hat{H}_e = \sum_{ij}^{N_{\text{so}}} h_{ij} \hat{a}_i^\dagger \hat{a}_j + \frac{1}{2} \sum_{ijkl}^{N_{\text{so}}} g_{ijkl} \hat{a}_i^\dagger \hat{a}_j^\dagger \hat{a}_l \hat{a}_k, \quad (1)$$

where  $\hat{a}_i^\dagger$  and  $\hat{a}_i$  are fermion creation and annihilation operators, and

$$h_{ij} = \int \psi_i^*(\mathbf{x}) \left( -\frac{1}{2} \nabla^2 - \sum_I \frac{Z_I}{|\mathbf{r} - \mathbf{R}_I|} \right) \psi_j(\mathbf{x}) d\mathbf{x}, \quad (2)$$

$$h_{ijkl} = \int \int \frac{\psi_i^*(\mathbf{x}_1) \psi_k^*(\mathbf{x}_2) \psi_j(\mathbf{x}_1) \psi_l(\mathbf{x}_2)}{r_{12}} d\mathbf{x}_1 d\mathbf{x}_2 \quad (3)$$

are values of one- and two-electron integrals written in a spin-orbital basis of  $\psi_j(\mathbf{x})$ ;  $\mathbf{x} = (\mathbf{r}, \sigma)$ . They were computed using the locally modified GAMESS-US<sup>5,6</sup> [ver. 30 SEP 2019 (R2)] program.

The electronic Hamiltonian (1) is converted to a qubit form by the Jordan–Wigner (JW) transformation<sup>3,7</sup> to obtain

$$\hat{H} = \sum_{k=1}^M C_k \hat{P}_k, \quad (4)$$

where  $C_k$  are coefficients inferred from the molecular integrals, and  $\hat{P}_k$  are Pauli strings (“words”), the products of Pauli elementary operators  $\sigma_j = x_j, y_j$ , or  $z_j$  acting on an individual  $j$ -th qubit,

$$P_k = \prod_{j \geq 0, j \in j(k)} \sigma_j. \quad (5)$$

As long as the molecular Hamiltonian is a *real* operator, which is always the case in the absence of a magnetic field, every  $P_k$  contains the *even* number of  $y_j$  factors.

The pairwise grouping of spin-orbitals was employed: the first orbital with  $\alpha$  (up) spin is mapped to the first qubit, followed by the first orbital with  $\beta$  spin, which is mapped to the second, etc. The advantage of using JW transformation is one-to-one correspondence between population of fermion spin-orbitals and states of qubits. We introduce a qubit reference vector

$$|0\rangle = \prod_{k=1}^{n_e} |\downarrow\rangle_k \times \prod_{k=1}^{N-n_e} |\uparrow\rangle_k, \quad (6)$$

where  $n_e$  is the number of electrons (equals to the number of *occupied* spin-orbitals), and



$N$  is the total number of qubits. Hence,  $(N - n_e)$  qubits correspond to *unoccupied* (virtual) orbitals. Together, employed occupied and virtual spin-orbitals constitute the complete active space (CAS) for the problem. If  $N$  is twice the size of the atomic basis, one deals with the full configurational interaction (FCI) problem, otherwise it is a complete active space self-consistent field (CASSCF)-like problem with the active space which is conveniently abbreviated as  $\text{CAS}(n_e, N)$ . It must be noted that the iQCC method with CAS other than the all electron/full basis (the FCI problem) is *not* equivalent to either the conventional CASSCF (which performs the full orbital optimization) or the complete active space configurational interaction (CASI) (which does not touch orbitals at all) problem. iQCC does not distinguish between orbital and CI-coefficient optimizations within the active space, but does not change orbitals outside CAS.

The state given by Eq. (6) represents a simple qubit product state—a special case of previously used qubit coherent states.<sup>8</sup> The new feature of the current iQCC implementation is that this state is fixed throughout iQCC iterations, see Sec. S1.5 for details.

## S1.2 Normal-ordered qubit Hamiltonians

The qubit Hamiltonian, Eq. (4), is a simple linear combination of Pauli words. Although this form is general, it does not offer any advantage for evaluation of the quantum-mechanical expectation values. It can be regrouped, however, as

$$\hat{H} = \hat{I}_0(\mathbf{z}) + \sum_{k>0} \hat{I}_k(\mathbf{z}) X_k, \quad (7)$$

which we call the “Ising decomposition”, and which is convenient to set up the iQCC method.  $\hat{I}_k(\mathbf{z})$  for  $k = 0, 1, \dots$  are qubit Hamiltonians which are the sum of Pauli words containing only  $\hat{z}$  Pauli elementary operators (“generalized Ising Hamiltonians”). All  $X_k$  are the Pauli  $X$ -strings. Namely,

$$X_k = \prod_{j \geq 0, j \in j(k)} \hat{x}_j. \quad (8)$$

To evaluate the mean values with operators in their Ising decomposition, we need a qubit reference vector [see Eq. (6)], and action rules for elementary Pauli operators  $\hat{z}_i$ :

$$\hat{z}_i |\downarrow\rangle_j = (1 - 2\delta_{ij}) |\downarrow\rangle_j \quad (9)$$

$$\hat{z}_i |\uparrow\rangle_j = |\uparrow\rangle_j \quad (10)$$

Note that any  $X$ -string operators have always *zero* matrix elements,  $\langle 0|X_k|0\rangle = 0$  for any  $|0\rangle$ , so that they are purely off-diagonal operators. The following identity holds (taking  $\hat{H}$  as an example):

$$\langle 0|\hat{H}|0\rangle = \langle 0|\hat{I}_0|0\rangle, \quad (11)$$

where  $\hat{I}_0$  is the corresponding operator from the Ising decomposition (7).

### S1.3 The qubit coupled cluster (QCC) Ansatz

In the current study we use a generic QCC form:

$$\hat{U}(\mathbf{t}) = \hat{U}(t_1, \dots, t_L) = \prod_{j=1}^L \exp\left(-it_j \hat{T}_j/2\right), \quad (12)$$

where  $t_j$  are amplitudes to be optimized,  $\hat{T}_j$  are generators, and  $L \leq 16$  is the number of them. The upper limit is dictated by the current implementation (see Sec. S1.5) and the hardware resources available; in general, computation costs increase *exponentially* with  $L$ .

### S1.4 QCC operator ranking

$\hat{T}_k$ , the generators of the QCC form, can be derived from  $X_k$  operators appearing in the Ising decomposition (7).<sup>9</sup> In particular, to convert a given  $X_k$  into  $T_k$  that is characterized by a

non-zero value of the energy gradient

$$\left. \frac{dE[T_k]}{dt} \right|_{t_k=0} = \frac{1}{2i} \langle 0 | [\hat{H}, \hat{T}_k] | 0 \rangle = \frac{1}{2} \Im \langle 0 | [\hat{H}, \hat{T}_k] | 0 \rangle, \quad (13)$$

one has to substitute the *odd* number of elementary  $\hat{x}_j$  operators in  $\hat{X}_k$  for their  $\hat{y}$  counterparts. Only such generators may have non-zero gradients and hence, change the total energy as they are purely *imaginary* operators. We always replace a single  $\hat{x}_j$  with the smallest possible  $j$  and call that choice “canonical”.

The energy expectation value at the  $i$ -th iQCC iteration,

$$E^{(i)}(t_1, \dots, t_L) = \langle 0 | (U^{(i)})^\dagger(t_1, \dots, t_L) \hat{H}^{(i-1)} U^{(i)}(t_1, \dots, t_L) | 0 \rangle, \quad (14)$$

depends on the ordering of generators in Eq. (12). We sort all possible generators [whose number is equal to the number of terms in the sum in the right-hand side of Eq. (7)] according to their “importance measure”. It can be an absolute gradient value, Eq. (13), the choice that were used in Ref. 10, or an absolute value of the optimal amplitude<sup>9</sup> – the current choice. For the sake of completeness, we derive the formula for the latter below. Consider the QCC form with a single generator  $\hat{T}$ :

$$\begin{aligned} E[\hat{T}](t) &= \langle 0 | \exp(it\hat{T}/2) \hat{H} \exp(-it\hat{T}/2) | 0 \rangle \\ &= \langle 0 | \hat{H} | 0 \rangle + \frac{\sin(t)}{2i} \langle 0 | [\hat{H}, \hat{T}] | 0 \rangle + \frac{1 - \cos(t)}{2} \langle 0 | (\hat{T} \hat{H} \hat{T} - \hat{H}) | 0 \rangle \end{aligned} \quad (15)$$

Identifying<sup>9</sup>

$$\omega = \frac{1}{2} |\langle 0 | [\hat{H}, \hat{T}] | 0 \rangle| = |\langle 0 | \hat{H} \hat{T} | 0 \rangle| \quad (16)$$

$$D = \langle 0 | \hat{T} \hat{H} \hat{T} - \hat{H} | 0 \rangle \quad (17)$$

we can write:  $E(t) = E_0 + \omega \sin(t) + D(1 - \cos t)/2$ , which gives the energy lowering of

$$\Delta E = D/2 - \sqrt{(D/2)^2 + \omega^2} \approx -\frac{\omega^2}{D} < 0 \text{ if } D > 0, \text{ when}$$

$$t = \arcsin \frac{2\omega}{\sqrt{D^2 + 4\omega^2}}. \quad (18)$$

If  $\hat{T} \equiv \hat{T}_k$  for some generator (*e.g.* canonical) derived from the Ising decomposition as described above, then the corresponding  $|t_k|$  is the sought-for importance measure. Additionally,

$$\omega_k = \left| \langle 0 | \hat{I}_k | 0 \rangle \right|, \quad (19)$$

where  $\hat{I}_k$  is taken from the Ising decomposition of the current Hamiltonian, Eq. (7).

When  $T_k$  are sorted in descending order (highest come first) according to the chosen importance measure, top  $L$  of them are selected for the QCC Ansatz, Eq. (12), for the next iteration. The remaining generators are used to set up the perturbative correction, see Ref. 9 for details.

## S1.5 Variational quantum eigensolver (VQE)-style energy optimization

Optimization of the QCC energy expression (14) is a non-linear optimization problem. We solved it on a classical computer with the aid of NLOpt optimization library.<sup>11</sup> Specifically, the low-storage BFGS algorithm<sup>a</sup> was employed. The non-linear energy functional (14) was implemented as a part of our quantum simulator; it is capable of evaluating energy values and corresponding gradients<sup>b</sup>.

Eq. (18) was used to provide the initial guess to amplitudes with  $\omega_k$  evaluated (along with correct signs) by Eq. (19). With such a choice of the initial amplitudes, the number of the objective function evaluations during optimization was less than 15. No additional constraints

<sup>a</sup>Implemented and posted online as a LGPL Fortran library by Ladislav Luksan.<sup>12</sup> The L-BFGS method itself is originated from Refs. 13 and 14.

<sup>b</sup>On real quantum hardware gradients can be efficiently evaluated using the parameter shift approach<sup>15</sup>

were applied, but the triplet energy functional was constructed by adding a penalty term

$$\mu\hat{W} = \mu \left( \hat{S}^2 - s(s+1)\hat{S}_z \right), \quad (20)$$

where  $\hat{S}^2$  and  $\hat{S}_z$  are the total spin squared operator and its  $z$  projection, respectively,  $s = 1$  is a spin quantum number for a triplet state, and  $\mu = 0.25$  is a penalty parameter, to the Hamiltonian,

$$\hat{H} \rightarrow \hat{H} + \mu\hat{W}. \quad (21)$$

We also added the penalty term with the same  $\mu$  and  $s = 0$  for the singlet state to obtain more correct gap values as the energy minima for penalized operators are close, but not identical to those for an un-penalized problem.<sup>16</sup>

Contrary to the previous studies, (*e.g.* Ref. 10), single-qubit (mean-field) optimizations were not performed, and the qubit reference state  $|0\rangle$  was fixed during iQCC iterations. The rationale was the following: the QCC form is flexible enough to include generators of a single-qubit transformations, which are simply  $\hat{T}_k = \hat{y}_k$ . Whenever such generators are necessary (which is determined by their large values of the important measure), they will be included into the QCC Ansatz automatically.

## S1.6 Hamiltonian dressing

Once the optimal values of amplitudes  $\mathbf{t}_{\text{opt}}$  are found, the iQCC program performs *dressing* of the current Hamiltonian. Below we show an elementary step of this transformation, which corresponds to  $L = 1$  in Eq. (12). For  $L > 1$  these steps are performed recursively. Dressing is a unitary transformation of the current Hamiltonian using the *optimal numerical* values of amplitude(s) at the current iteration:

$$\hat{H}^{(i+1)} = \left( U^{(i)} \right)^\dagger (t_{\text{opt}}) \hat{H}^{(i)} U^{(i)}(t_{\text{opt}}) = \hat{H}^{(i)} - \frac{i}{2} \sin(t_{\text{opt}}) [\hat{H}^{(i)}, \hat{T}] + \frac{1 - \cos t_{\text{opt}}}{2} \left( \hat{T} \hat{H}^{(i)} \hat{T} - \hat{H}^{(i)} \right). \quad (22)$$

New terms in  $\hat{H}^{(i+1)}$  come from the second, commutator term in the right-hand side of Eq. (22), because an operator  $(\hat{T}\hat{H}\hat{T} - \hat{H})$  shares the same terms with  $\hat{H}$  for *any* Pauli word  $\hat{T}$ . “On average” an arbitrary  $\hat{T}$  commutes with a half of terms in  $\hat{H}$ , so after the dressing the number of terms in  $\hat{H}^{(i+1)}$  increases by a factor of  $3/2$ .<sup>10</sup> In a more general case,  $L > 1$ , this translates into  $(3/2)^L$ , and for  $K$  iQCC iterations into  $(3/2)^{KL}$ . Thus, *formally*, the iQCC method is exponentially complex both in the size of the QCC Ansatz and the number of iterations. However, all new terms are multiplied by some products of  $\sin(t_{k,\text{opt}}) < 1$  for  $1 \leq k \leq L$ . Additionally, for  $L > 1$   $\sin(t_{k,\text{opt}})$  decrease with  $L$  since  $t_{k,\text{opt}}$  correlate with decreasing values of the importance measure, see Sec. S1.4. Also, *maximal*  $\sin(t_{\text{opt}})$  tends to decrease in the course of iQCC iterations. As a result, the dressed Hamiltonians accumulate a lot of terms those numerical values are tiny, frequently many orders of magnitudes smaller than the accuracy of the initial Hamiltonian coefficients, which, in turn, is determined by the accuracy of molecular integrals. Moreover, despite the abundance of such terms their cumulative contribution to the ground-state energy is negligibly small. This situation is somewhat known to the quantum community; for example, Ref. 17 coined the term “configuration interaction (CI) deadwood”. Dropping such terms, however, not only limits the growth (proliferation of terms) of dressed Hamiltonians, but drastically changes the *asymptotics* of such growth. As can be seen from Fig. 2c of the main text, the number of numerically *significant* terms quickly deviates from the expected exponential asymptotics. By fitting the Hamiltonian size as a function of the iteration number, we found that at late iterations the actual asymptotics is close to low-power polynomial, for example,  $M^{1.608}$  for data on Fig 2c. This suggests that with our “canonical” choice of generators, amplitudes of less than two generators are correlated, and the second-order Epstein-Nesbet perturbation theory (see Ref. 9) may be very accurate. Indeed, for our materials we observed that the most of the QCC top-ranked generators were originated from the initial (bare, un-dressed) double fermionic excitations; rarely we saw single- and higher-order composite excitations that results from dressing. This implies, however, that the iQCC method generates composite (*e.g.* high-order) excitations and

combines them with the original double fermionic excitations whenever necessary. In contrast to other methods proposed in the literature, such as ADAPT-VQE<sup>18</sup> or a (generalized) unitary coupled cluster (UCC) ones,<sup>4,19–24</sup> no preliminary selection of a “generator pool” or a generators’ excitation rank is required to include energetically important generators into Ansätze. The Hamiltonian itself naturally drives the ground-state optimization, which allows to consider the iQCC method as a genuinely black-box electronic-structure method.

It is also clear that for many molecular systems theoretical (exponential) complexity of the iQCC procedure has little relevance to the actual complexity, significantly widening the potential applicability of the iQCC method to realistic systems.

## S2 Active orbital selection

For generating the triplet state Hamiltonians, we used the basis of restricted open-shell Hartree–Fock molecular orbitals (MOs). Namely, one- and two-electron molecular integrals in Eq. (1) were computed using the restricted open-shell Hartree–Fock (ROHF) orbitals. This choice was largely unproblematic for all materials with an exception of Ir(ppz)<sub>3</sub>: for this molecule we found an alternative set of ROHF orbitals with lower energy, namely,  $-1465.167\,381\,E_h$  *vs.*  $-1456.151\,315\,E_h$  found by GAMESS starting from the “Huckel” guess. New orbitals were generated by running the unrestricted Hartree–Fock (UHF) calculations first; UHF natural orbitals were prepared and used subsequently as a guess for ROHF calculations.

The space of active MOs was chosen as follows: the lowest 18 occupied orbitals below the Fermi level and 18 virtual orbitals above it were selected. In parallel UHF calculations we found that 18 natural UHF orbitals<sup>25</sup> below the Fermi level had occupation numbers within a range 1.998–1.000, while 18 above had occupation in a range 1.000–0.0017. Hence, ROHF orbitals that lie below HOMO-18 are likely to span the same orbital space as their UHF counterparts (because the all have occupation numbers close to 2), and orbitals above

Table S1:  $\langle \hat{S}^2 \rangle$  values for the UHF determinant, an ideal value is 2.

Material	Value
Ir(ppz) <sub>2</sub> (F <sub>2</sub> ppy)	3.892
Ir(ppz) <sub>3</sub>	3.587
Ir(F <sub>2</sub> ppz) <sub>3</sub>	2.412
Ir(F <sub>2</sub> ppz) <sub>2</sub> (F <sub>2</sub> ppy)	3.293
Ir(F <sub>2</sub> ppz) <sub>2</sub> (ppy)	2.715
Ir(ppy) <sub>3</sub>	4.879
Ir(ppz) <sub>2</sub> (ppy)	4.933
Ir(pmb) <sub>3</sub>	3.976
Ir(F <sub>2</sub> ppy) <sub>3</sub>	4.411

constitute the “spin-polarized” subsystem, which must be a part of the active space.<sup>26</sup> An additional benefit of using ROHF orbitals is that, the initial QCC energy matches the ROHF value if a qubit reference vector is chosen as in Eq. (6).

Likewise, the choice of virtual orbitals for CAS is rather simple for the studied materials in the selected double-zeta basis set (6-31G\* basis set<sup>27</sup> and its pseudopotential partner for the Ir center<sup>28</sup>). All orbitals are ordered by their Hartree–Fock canonical energies,  $\epsilon_i < 0$  for the valence and  $\epsilon_i > 0$  for the virtual ones. In a double-zeta basis each occupied orbital is usually paired with at least one virtual, so mechanical including lowest virtual orbitals into the active space in general leads to a correct description of correlation effects. If, for example, extended basis sets with multiple *diffuse* basis functions were used, there would be numerous *Rydberg* states, which are weakly bound (or scattered) states with orbital energies close to 0 and having virtually zero correlation contributions<sup>c</sup>. They would pollute the virtual space making the CAS selection difficult.

### S3 Spin contamination of the UHF wave function

Notwithstanding what was said above about the electronic correlation captured by the QCC Ansatz, investigated molecules in their triplet states *cannot* be considered as weakly correlated.

<sup>c</sup>Rydberg states can be largely avoided if additional (polarization) functions are systematically added by a procedure described in Ref. 29. It is demonstrated there that augmentation of a split-valence basis set with only one *d* function per atom leaves appreciable (23%) basis set error. However, since we seek for the singlet-triplet energy *difference*, error compensation seems to guarantees reasonably accurate differences in a chosen singly-augmented 6-31G\* basis set.



Table S1 shows that the single-determinant description of the triplet state is severely flawed, showing strong spin contamination in the UHF description of those molecules.

## S4 The Jahn-Teller effect in studied materials

All studied materials are susceptible to the Jahn-Teller<sup>30</sup> effect in their triplet states. Below we present a concise study of the Jahn-Teller effect in the  $^3\text{Ir}(\text{ppy})_3$  molecule.<sup>31</sup> We have performed configuration-interaction singles (CIS) calculations of triplet states in a geometrical configuration of the *singlet* state which has  $C_3$  symmetry. Three almost degenerate triplet states were found<sup>d</sup>, see Table S2.

The Jahn-Teller effect leads to a geometrical distortion of the  $^3\text{Ir}(\text{ppy})_3$  molecule and lifts the electronic degeneracy. As a result, three energetically equivalent lower-symmetry minima emerge on a largely flat, strongly anharmonic potential energy surface (PES). These minima are connected by low barriers, so that the molecule is floppy and exhibit large-amplitude motion even at low temperature. This also contributes to the difficulties in geometry optimization as changing the level of theory and various convergence thresholds lead to substantial changes in the optimized structure. It appears that *all* materials share this floppiness, and it is related to the close-to-octahedral coordination of the Ir center and ensuing Jahn-Teller distortion. From a practical standpoint, this causes the optimal geometrical parameters of triplets to be sensitive to the chosen functional. To minimize the impact of a functional, structures were optimized using CAM-B3LYP<sup>32</sup> functional with the LANL2def-DZV basis set<sup>33,34</sup> using the unrestricted formalism.

<sup>d</sup> $C_3$  group has no three-fold degenerate irreducible representations, hence, at least one degeneracy is either accidental or actually has a very small yet finite gap. This is not surprising since *local* coordination of the Ir atom is close to octahedral, and the  $O_h$  group has there-fold degenerate irreducible representations.

Table S2: Energy (in  $E_h$ ) and the dominant orbital excitations for of the lowest states in the triplet manifold for  $\text{Ir}(\text{ppy})_3$  in its  $S_0$  configuration. The Fermi level is between orbitals 130 and 131, the reference energy is  $E(\text{RHF}) = -1531.035\,557\,E_h$ .

State	Energy	Transition characteristics		
		From orbital	To orbital	Coefficient
$1^3\text{Ir}(\text{ppy})_3$	-1530.924 970	126	131	0.2180
$2^3\text{Ir}(\text{ppy})_3$	-1530.924 862	127	131	0.2166
$3^3\text{Ir}(\text{ppy})_3$	-1530.924 635	130	131	0.2553

## S5 Details of the Computational and Experimental Methods

All density-functional theory (DFT) calculations were run on a Westgrid high-performance computing server. Each calculation was run on a single server node – two-socket Intel E5-2683 v4 Broadwell@2.1GHz, 125 GB RAM, 960 GB SATA SSD – with allocated resources of 16 processor cores and a maximum of 64 GB RAM. Some calculations that required more memory (*e.g.* second-order Møller–Plesset perturbation theory (MP2)) were run with a maximum of 200 GB RAM. The actual memory use varied depending on the compound under study and a type of calculations performed. Values of  $T_1 \rightarrow S_0$  transition energy for all methods employed are listed in Table S3.

The iQCC simulations were run on Ev3 Microsoft Azure compute instances that have Intel Xeon E5-2673 v4 Broadwell@2.3 GHz, 432 GB RAM, and 864 GB SSD. The iQCC method was implemented in Julia language ver. 1.5<sup>35</sup> and ran mostly serially, with several non-critical parts parallelized with thread parallelization available in Julia (`Threads.@parallel` with `nproc = 16–32`). All simulations finished between 200–480 CPU hours per simulation. All simulations were run until the energy changes were about  $1 \times 10^{-5} E_h$ , which typically required  $\sim 75$  iterations with 8 top-rank generators selected at each iteration ranked by Eq. (18) (see Sec. S1.4).

To assess the quantum circuit specifications of the QCC Ansatz, ProjectQ was used to generate circuits and resource estimates.<sup>36</sup> Each of the nine Ir(III) complexes had a total

of 600 entanglers optimized and it was observed that most of the high ranking entanglers were either 2-qubit or 4-qubit operators. These entanglers were decomposed using the Time Evolution operator in ProjectQ to generate a proposed quantum circuit. In this instance, the longest circuit had a total of 3600 CNOT gates and 600 RZ rotation gates. At the time of writing this value exceeds what is currently possible on quantum hardware.

Empirical values for the  $T_1 \rightarrow S_0$  transitions for the nine Ir (III) complexes were taken from the work of Sajoto *et al.*<sup>37</sup> As calibration, the phosphorescence spectrum of Ir(ppy)<sub>3</sub> was confirmed with an Edinburgh Instruments FS5 spectrofluorometer using the SC-70 sample module. The spectrum was measured by dissolving Ir(ppy)<sub>3</sub> in 2-methyltetrahydrofuran at 0.05 mg ml<sup>-1</sup> mg/mL and cooling to 77 K in a quartz EPR tube, then exciting with 365 nm light. The value obtained for the  $T_1 \rightarrow S_0$  transition matched exactly ( $\delta\lambda < 1$  nm) with Sajoto.<sup>37</sup>

Table S3:  $T_1 \rightarrow S_0$  transitions of the Ir (III) complexes in eV dependent on computational method

Method	Ir(ppv) <sub>3</sub>	Ir(F <sub>2</sub> ppv) <sub>3</sub>	Ir(ppz) <sub>2</sub> (ppv)	Ir(F <sub>2</sub> ppz) <sub>2</sub> (ppv)	Ir(ppz) <sub>2</sub> (F <sub>2</sub> ppv)	Ir(F <sub>2</sub> ppz) <sub>2</sub> (F <sub>2</sub> ppv)	Ir(ppz) <sub>3</sub>	Ir(F <sub>2</sub> ppz) <sub>3</sub>	Ir(pmb) <sub>3</sub>
ROHF/RHF	3.497	2.891	3.018	2.758	2.730	2.871	3.001	2.979	2.666
UHF/RHF	1.990	2.607	2.028	1.643	1.532	2.859	2.122	2.256	2.571
RO-B3LYP/R-B3LYP	Failed	Failed	Failed	2.434	Failed	2.549	Failed	2.809	2.616
U-B3LYP/R-B3LYP	2.630	2.454	2.484	2.356	2.247	2.471	2.622	2.734	2.560
RO-PBE/RO-PBE	3.993	4.465	5.375	2.264	5.298	2.369	4.250	4.752	3.975
RO-CAMB3LYP/R-CAMB3LYP	3.028	2.724	2.747	2.610	2.473	2.729	2.853	2.973	2.802
U-CAMB3LYP/R-CAMB3LYP	3.133	2.583	2.629	2.483	2.331	2.582	2.730	2.841	2.715
RO-LC-wPBE/R-LC-wPBE	3.119	2.833	2.760	2.704	2.496	2.828	2.916	3.063	2.902
U-LC-wPBE/R-LC-wPBE	3.431	2.592	2.599	2.479	2.273	2.579	2.745	2.844	2.776
TDDFT R-B3LYP	2.502	2.294	2.288	2.213	1.980	2.302	2.400	2.525	2.393
TDDFT + TDA R-B3LYP	2.549	2.430	2.381	2.334	2.046	2.450	2.492	2.681	2.470
TDDFT R-CAMB3LYP	2.724	2.228	2.384	2.150	2.330	2.212	2.608	2.459	2.586
TDDFT + TDA R-CAMB3LYP	2.958	2.556	2.717	2.467	2.536	2.555	2.852	2.792	2.776
TDDFT R-LC-wPBE	2.492	1.938	2.121	1.826	2.267	1.907	2.536	2.202	2.510
TDDFT + TDA R-LC-wPBE	3.087	2.576	2.814	2.490	2.784	2.568	3.006	2.828	2.967
ROMP2/RMP2	8.901	2.926	3.611	2.708	2.317	2.911	3.017	3.495	3.369
UMP2/MP2	8.901	5.615	4.534	6.899	5.096	5.322	5.170	4.384	5.629
iQCC	2.858	2.842	2.101	2.693	2.337	2.710	2.461	3.109	2.951
iQCC + PT	2.901	9.899	2.820	2.948	2.782	3.064	2.969	3.320	3.070

## References

- (1) Helgaker, T.; Jorgensen, P.; Olsen, J. *Molecular Electronic-structure Theory*; Wiley, 2000.
- (2) Abrams, D. S.; Lloyd, S. Simulation of Many-Body Fermi Systems on a Universal Quantum Computer. *Phys. Rev. Lett.* **1997**, *79*, 2586–2589.
- (3) Aspuru-Guzik, A.; Dutoi, A. D.; Love, P. J.; Head-Gordon, M. Simulated Quantum Computation of Molecular Energies. *Science* **2005**, *309*, 1704–1707.
- (4) Peruzzo, A.; McClean, J.; Shadbolt, P.; Yung, M.-H.; Zhou, X.-Q.; Love, P. J.; Aspuru-Guzik, A.; O’Brien, J. L. A variational eigenvalue solver on a photonic quantum processor. *Nat. Commun.* **2014**, *5*, 4213.
- (5) Schmidt, M. W.; Baldridge, K. K.; Boatz, J. A.; Elbert, S. T.; Gordon, M. S.; Jensen, J. H.; Koseki, S.; Matsunaga, N.; Nguyen, K. A.; Su, S. J.; Windus, T. L.; Dupuis, M.; Montgomery, J. General Atomic and Molecular Electronic Structure System. *J. Comput. Chem.* **1993**, *14*, 1347–1363.
- (6) Gordon, M. S.; Schmidt, M. W. In *Theory and Applications of Computational Chemistry. The first forty years*; Dykstra, C. E., Frenking, G., Kim, K. S., Scuseria, G. E., Eds.; Elsevier: Amsterdam, 2005; pp 1167–1189.
- (7) Jordan, P.; Wigner, E. Über das Paulische Äquivalenzverbot. *Z. Phys.* **1928**, *47*, 631–651.
- (8) Ryabinkin, I. G.; Yen, T.-C.; Genin, S. N.; Izmaylov, A. F. Qubit Coupled Cluster Method: A Systematic Approach to Quantum Chemistry on a Quantum Computer. *J. Chem. Theory Comput.* **2018**, *14*, 6317–6326.
- (9) Ryabinkin, I. G.; Izmaylov, A. F.; Genin, S. N. A posteriori corrections to the iterative qubit coupled cluster method to minimize the use of quantum resources in large-scale calculations. *Quantum Sci. Technol.* **2021**, *6*, 024012.

- (10) Ryabinkin, I. G.; Lang, R. A.; Genin, S. N.; Izmaylov, A. F. Iterative Qubit Coupled Cluster Approach with Efficient Screening of Generators. *J. Chem. Theory Comput.* **2020**, *16*, 1055–1063, PMID: 31935085.
- (11) Johnson, S. G. The NLOpt nonlinear-optimization package. on-line, 2020; <https://github.com/stevengj/nlopt>, Julia package at <https://github.com/JuliaOpt/NLOpt.jl>.
- (12) Luksan, L. online, [www.uivt.cas.cz/~luksan/subroutines.html](http://www.uivt.cas.cz/~luksan/subroutines.html).
- (13) Nocedal, J. Updating quasi-Newton matrices with limited storage. *Math. Comput.* **1980**, *35*, 773–782.
- (14) Liu, D. C.; Nocedal, J. On the limited memory BFGS method for large scale optimization. *Math. Program.* **1989**, *45*, 503.
- (15) Schuld, M.; Bergholm, V.; Gogolin, C.; Izaac, J.; Killoran, N. Evaluating analytic gradients on quantum hardware. *Phys. Rev. A* **2019**, *99*, 032331.
- (16) Nocedal, J.; Wright, S. J. *Numerical Optimization*, 2nd ed.; Springer Series in Operations Research and Financial Engineering; Springer New York, 2006.
- (17) Ivanic, J.; Ruedenberg, K. Identification of deadwood in configuration spaces through general direct configuration interaction. *Theor. Chem. Acc.* **2001**, *106*, 339–351.
- (18) Grimsley, H. R.; Economou, S. E.; Barnes, E.; Mayhall, N. J. An adaptive variational algorithm for exact molecular simulations on a quantum computer. *Nat. Commun.* **2019**, *10*, 3007.
- (19) McClean, J. R.; Romero, J.; Babbush, R.; Aspuru-Guzik, A. The theory of variational hybrid quantum-classical algorithms. *New J. Phys.* **2016**, *18*, 023023.
- (20) O’Malley, P. J. J. et al. Scalable Quantum Simulation of Molecular Energies. *Phys. Rev. X* **2016**, *6*, 031007.

- (21) Romero, J.; Babbush, R.; McClean, J. R.; Hempel, C.; Love, P. J.; Aspuru-Guzik, A. Strategies for quantum computing molecular energies using the unitary coupled cluster ansatz. *Quantum Sci. Technol.* **2018**, *4*, 014008.
- (22) Hempel, C.; Maier, C.; Romero, J.; McClean, J.; Monz, T.; Shen, H.; Jurcevic, P.; Lanyon, B. P.; Love, P.; Babbush, R.; Aspuru-Guzik, A.; Blatt, R.; Roos, C. F. Quantum Chemistry Calculations on a Trapped-Ion Quantum Simulator. *Phys. Rev. X* **2018**, *8*, 031022.
- (23) Nam, Y. et al. Ground-state energy estimation of the water molecule on a trapped ion quantum computer. *arXiv e-prints* **2019**, 1902.10171.
- (24) Lee, J.; Huggins, W. J.; Head-Gordon, M.; Whaley, K. B. Generalized Unitary Coupled Cluster Wave functions for Quantum Computation. *J. Chem. Theory Comput.* **2019**, *15*, 311–324.
- (25) Pulay, P.; Hamilton, T. P. UHF natural orbitals for defining and starting MC-SCF calculations. *J. Chem. Phys.* **1988**, *88*, 4926–4933.
- (26) Abrams, M. L.; Sherrill, C. D. Natural orbitals as substitutes for optimized orbitals in complete active space wavefunctions. *Chem. Phys. Lett.* **2004**, *395*, 227–232.
- (27) Hehre, W. J.; Ditchfield, R.; Pople, J. A. Self—Consistent Molecular Orbital Methods. XII. Further Extensions of Gaussian—Type Basis Sets for Use in Molecular Orbital Studies of Organic Molecules. *J. Chem. Phys.* **1972**, *56*, 2257–2261.
- (28) Stevens, W. J.; Krauss, M.; Basch, H.; Jasien, P. G. Relativistic compact effective potentials and efficient, shared-exponent basis sets for the third-, fourth-, and fifth-row atoms. *Can. J. Chem.* **1992**, *70*, 612–630.
- (29) Rappoport, D.; Furche, F. Property-optimized Gaussian basis sets for molecular response calculations. *J. Chem. Phys.* **2010**, *133*, 134105.

- (30) Majumdar, D.; Samanta, P. N.; Roszak, S.; Nguyen, M. T.; Leszczynski, J. Jahn-Teller and Pseudo Jahn-Teller Effects: Influences on the Electronic Structures of Small Transition, Main Group and Mixed Metal Clusters. *Structural Chemistry* **2020**, *31*, 7.
- (31) Fine, J.; Diri, K.; Krylov, A. I.; Nemirow, C.; Lu, Z.; Wittig, C. Electronic structure of tris(2-phenylpyridine)iridium: electronically excited and ionized states. *Mol. Phys.* **2012**, *110*, 1849–1862.
- (32) Yanai, T.; Tew, D. P.; Handy, N. C. A new hybrid exchange-correlation functional using the Coulomb-attenuating method (CAM-B3LYP). *Chem. Phys. Lett.* **2004**, *393*, 51–57.
- (33) Hay, P. J.; Wadt, W. R. Ab initio effective core potentials for molecular calculations. Potentials for K to Au including the outermost core orbitals. *J. Chem. Phys.* **1985**, *82*, 299–310.
- (34) Roy, L. E.; Hay, P. J.; Martin, R. L. Revised Basis Sets for the LANL Effective Core Potentials. *J. Chem. Theory Comput.* **2008**, *4*, 1029–1031, PMID: 26636355.
- (35) Bezanson, J.; Edelman, A.; Karpinski, S.; Shah, V. Julia: A Fresh Approach to Numerical Computing. *SIAM Rev.* **2017**, *59*, 65–98.
- (36) Steiger, D. S.; Häner, T.; Troyer, M. ProjectQ: an open source software framework for quantum computing. *Quantum* **2018**, *2*, 49.
- (37) Sajoto, T.; Djurovich, P. I.; Tamayo, A. B.; Oxgaard, J.; Goddard, W. A.; Thompson, M. E. Temperature Dependence of Blue Phosphorescent Cyclometalated Ir(III) Complexes. *J. Am. Chem. Soc.* **2009**, *131*, 9813–9822.